

Spatiotemporal dynamics of quantum-well excitons

Hui Zhao, B. Dal Don, S. Moehl, and H. Kalt

Institut für Angewandte Physik, Universität Karlsruhe, D-76128 Karlsruhe, Germany

K. Ohkawa and D. Hommel

Institut für Festkörperphysik, Universität Bremen, D-28334 Bremen, Germany

(Received 12 July 2002; revised manuscript received 9 October 2002; published 14 January 2003)

We investigate the lateral transport of excitons in ZnSe quantum wells by using time-resolved micro-photoluminescence enhanced by the introduction of a solid immersion lens. The spatial and temporal resolutions are 200 nm and 5 ps, respectively. Strong deviation from classical diffusion is observed up to 400 ps. This feature is attributed to the hot-exciton effects, consistent with previous experiments under cw excitation. The coupled transport-relaxation process of hot excitons is modeled by Monte Carlo simulation. We prove that the two basic assumptions typically accepted in photoluminescence investigations on excitonic transport, namely, (i) the classical diffusion model as well as (ii) the equivalence between the temporal and spatial evolution of the exciton population and of the measured photoluminescence, are not valid for low-temperature experiments.

DOI: 10.1103/PhysRevB.67.035306

PACS number(s): 78.47.+p, 78.67.De, 78.55.Et

I. INTRODUCTION

Real-space transport of excitons in semiconductor is an important aspect of excitonic dynamics and plays an essential role in many optoelectronic applications. In a quantum-well (QW) structure, the excitons are confined in the QW plane by the potential barriers. The two-dimensional lateral transport of excitons in a number of semiconductor QW structures has been extensively studied during the past two decades by several optical techniques, e.g., transient grating, pump-probe, and photoluminescence (PL). In transient-grating experiments, a spatially periodic distribution of carrier density is generated by the interference of two laser pulses with different angles of incidence. The decay of this periodic distribution is then detected by the diffraction of a third pulse, and the diffusivity can be deduced from this decay.¹⁻⁷ In pump-probe measurements, an intense laser pulse is used to generate excitons, in which distribution is then detected by measuring the absorption of a delayed and much weaker probe beam. Scanning the probe beam with respect to the pump beam, one can obtain information on excitonic transport.⁸⁻¹³

Different from these nonlinear techniques, experiments based on PL can be performed in the low-density regime, where the interactions between carriers are negligible. This makes the interpretation of the experimental results and the deduction of the physics on exciton-environment coupling more straightforward. Two types of PL-based methods have been developed during the last decade. In time-of-flight experiments, the sample surface is covered by masks. Small holes are etched on this cover to transmit the excitation laser beam and the luminescence. The decay of the PL from the hole after a pulsed excitation can be attributed to both the radiative decay and the transport of excitons out of the hole, i.e., out of the detection window. Since the radiative decay can be measured independently by using samples without mask, information on transport can be deduced by modeling the PL decay by, normally, diffusion equation.¹⁴⁻²⁰ The other method is PL imaging, in which the spatial profiles of the

luminescence are measured directly, e.g., by a microscope.²¹⁻²⁸ Extensive information about the carrier diffusivity, mobility, and diffusion length has been extracted based on these two methods.

In these optical investigations based on PL, excitons are excited by laser photons with an excess energy E_{excess} of typically several tens to several hundreds of meV.¹⁴⁻²⁸ Despite the possibility that the transport can happen when the excitons are still hot, i.e., with high kinetic energy, the hot-exciton effects are typically neglected in this kind of studies. For the measurements performed at room temperature,²⁵⁻²⁸ hot-exciton effects are less pronounced due to fast relaxation. However, for low-temperature PL experiments with a rather high E_{excess} ,¹⁴⁻²⁴ the relaxation can take several hundreds of picoseconds.²⁹ If hot excitons play a role in the transport process, two basic assumptions of these PL experiments are questionable. The first problem is the validity of the diffusion equation in describing the transport process. During the relaxation, the kinetic energy and the group velocity of the hot excitons are decreasing. Thus, the transport during relaxation cannot be described as diffusion with a constant diffusivity. Second, the measured temporal and spatial evolutions of the PL are *not* equivalent to that of the exciton population. Due to the negligible photon momentum, the PL can only be used to monitor the cold excitons that have small enough momentum to be able to couple to a photon (see, e.g., Ref. 30). The hot excitons are invisible in these techniques. For this reason, the spatiotemporal evolution of the total exciton population including hot excitons can be quite different from that directly deduced from these experiments.

In this paper, we show that these two problems have to be accounted for in typical PL investigations on the transport of QW excitons. By performing temporally resolved micro-PL and Monte Carlo simulation, we investigate the excitonic transport in ZnSe QW's. Strong deviation from classical diffusion on a time scale of several hundreds of picoseconds is observed in the low-temperature experiments and is attributed to a persistent hot-exciton population. From the simulation, we obtain the spatiotemporal evolution of the total ex-

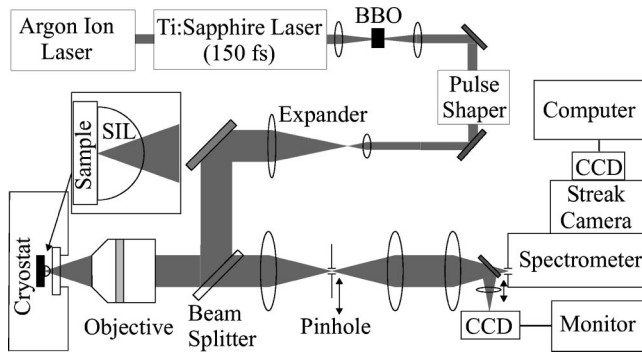


FIG. 1. Temporally resolved micro-photoluminescence enhanced by introducing SIL.

citon population and find a pronounced difference from that directly deduced from the PL.

II. EXPERIMENT

The experimental setup is a time-resolved micro-PL (μ -TRPL) enhanced by introducing a solid immersion lens (SIL). The spatial and temporal resolutions are 200 nm and 5 ps, respectively. Figure 1 shows schematically the configuration. The laser system including an Argon-ion laser and a Ti:Sapphire laser with double frequency by Beta Barium Borate (BBO) crystal generates tunable blue laser pulses of 150 fs with a repetition rate of 76 MHz. The pulse shaper reduces its spectral width to 0.2 meV. The beam is then spatially expanded to fit the diameter of the objective (magnification $20\times$, numerical aperture = 0.4), and focused on the sample surface. The luminescence is collected by the same objective, i.e., confocal configuration, and focused on the image plane of the microscope. A set of pinholes with different sizes is installed in this plane, achieving local detection. By moving the pinhole in the image plane, one can scan the detection spot with respect to the excitation spot in a well-defined way. The signal transmitting the pinhole is then spectrally resolved by a spectrometer, temporally resolved by a streak camera and recorded by a charge-coupled device (CCD). Additionally, a shiftable set of mirror and lens is installed in front of the spectrometer, reflecting and focusing the light to another CCD camera connected with a monitor. This configuration achieves a direct imaging of the sample surface on the monitor, thus ensures fine alignments of the laser beam, the objective, and the pinhole.

The high spatial resolution is achieved by using a hemispherical SIL made of ZrO_2 with refractive index of 2.16.³¹ The SIL is adhesively fixed to the sample surface. The diameter of the SIL is chosen to be 1 mm, which is large enough for giving a sufficient field of view, but still small enough to be stuck on the sample surface adhesively even in vertical configuration. The SIL enhances not only the spatial resolution by about two times due to the increased refractive index of the media outside the sample, but also the collection efficiency by more than five times due to a larger collection angle.³² These enhancements are of crucial importance for the current investigation. All measurements are performed at a sample temperature of 10 K.

Two ZnSe multiple-QW samples with different periods as

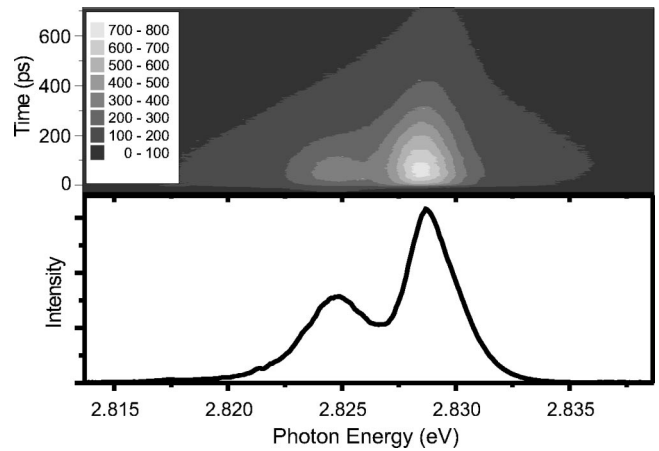


FIG. 2. Time-integrated (lower panel) and time-resolved (upper panel) photoluminescence spectra.

well as different barrier materials are studied. Since similar transport properties are observed in both samples, we focus here on the study of a ten-period ZnSe/ZnMgSSe multiple QW with 8 nm well width and 11 nm barrier width grown by molecular-beam epitaxy. Figure 2 shows time-integrated (lower panel) and time-resolved (upper panel) PL spectra of this sample excited by continuous-wave (cw) laser or pulsed laser, respectively. In both cases, the energy of the excitation photon is chosen to be 2.9013 eV. The heavy-hole exciton resonance is observed at 2.8287 eV with a linewidth of 2.9 meV. The rise time and decay time of this peak is measured as 65 ps and 205 ps, respectively. The lower-energy peak is attributed to charged excitons and is not examined here.

The μ -TRPL spectra are measured by moving the pinhole in the image plane, thus scanning the detection spot (450 nm in diameter, defined by the pinhole size) with respect to the fixed excitation spot. From these spectra, we obtain the temporal evolution of the spatial profile of heavy-hole exciton luminescence. The detection window used in this extraction is a small spectral region around the excitonic resonance. Figure 3 shows several PL profiles measured at a set of times after a pulsed-laser excitation. The photon energy of the laser is 2.9013 eV. The excitation power is less than $1 \mu W$, ensuring the condition of a low exciton density. The expansion of the PL profile that originates from the real-space transport of excitons is clearly observed.

III. MONTE CARLO SIMULATION

Monte Carlo (MC) simulations³³ have been successfully applied in investigations on carrier dynamics in semiconductor QW's.³⁴⁻⁴¹ In the present study, we use the MC method to simulate the laser excitation, excitonic transport, relaxation, and recombination processes. The model used for the simulation is based on the solid understanding of the hot-exciton formation and relaxation processes in ZnSe QW. After a laser excitation with a suitable photon energy, an electron-hole pair is excited in the continuum states. Generally, the electron-hole pair may (i) rapidly form a hot exciton with large center-of-mass wave vector, followed by hot-exciton relaxation, or (ii) dissociate into individual carriers

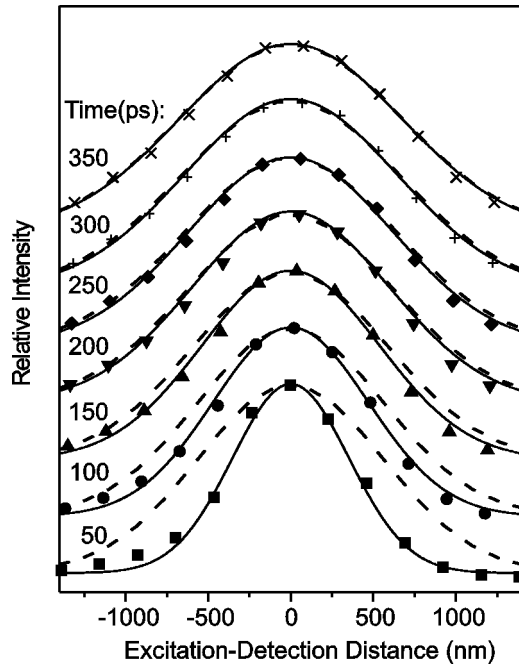


FIG. 3. Temporal evolution of the PL profile and of the exciton population profile. Points with different shapes: The PL profiles at different times after the excitation measured by scanning the pin-hole. Solid (dashed) lines: The corresponding PL (total exciton population) profiles obtained by the Monte Carlo simulation.

that relax to their band minima separately. In GaAs semiconductor structures, both theoretical and experimental studies have revealed a fast exciton-formation process following the excitation if the excess energy of the excitation is large enough for a LO-phonon emission of the excited electron-hole pair.^{42–47} In polar II-VI QW's, the LO-phonon-assisted exciton formation is as fast as sub-picosecond due to the strong Fröhlich coupling and thus dominates over the dissociation process. This has been verified by the experimental observations of hot-exciton luminescence in these structures.^{48–50} Our previous investigations on hot-exciton luminescence in ZnSe QW's by temporally resolved²⁹ or spatially resolved⁵¹ LO-phonon-sideband (PSB) spectroscopy as well as the observation of a pronounced LO-phonon cascade in PL excitation spectrum⁵² also confirm the dominant role of this fast exciton-formation process. Thus, in the simulation, we neglect the dissociation process and assume that all of the excited electron-hole pairs form excitons by the LO-phonon emission.

In the case when the hot exciton is formed with a center-of-mass kinetic energy E_k larger than the LO-phonon energy ($E_{LO} = 31.8$ meV in ZnSe QW), it relaxes rapidly toward its band minimum by LO-phonon emissions on a time scale of 100 fs, until $E_k < E_{LO}$.⁵² Then the rest of the relaxation is achieved by the much slower acoustic-phonon emission, and continues over several hundreds of picoseconds.²⁹ Since the LO-phonon-assisted formation and relaxation are much faster than the rest of the relaxation process, as a good approximation we can neglect the transport during the former processes. So the physical process in our experiment and, thus, in the model used for the simulation can be simplified

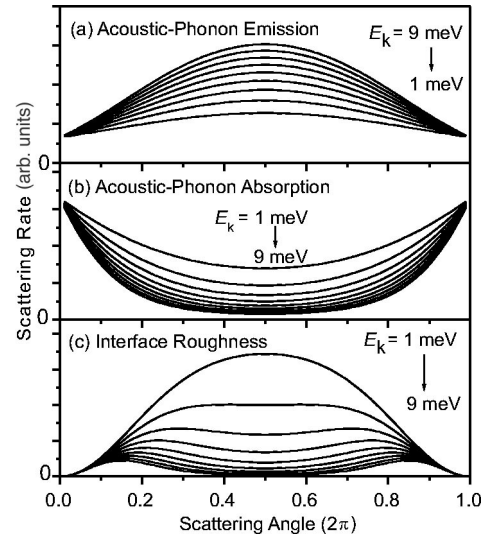


FIG. 4. Differential scattering rates of acoustic-phonon emission (a), acoustic-phonon absorption (b), and interface-roughness scattering (c) as function of scattering angle for several exciton kinetic energies E_k from 1 to 9 meV.

as follows: The laser pulse generates hot excitons with $E_k = E_{\text{excess}} - nE_{LO}$. In our experiment, $E_{\text{excess}} = 72.6$ meV, so $n = 2$ and $E_k = 9$ meV. The initial spatial distribution of the excitons is defined by the profile of the laser spot. After the generation, the hot excitons travel in real space and relax in energy space simultaneously until it recombines at $E_k \approx 0$. The radiative recombination induces the PL.

The scattering processes included in our simulation are acoustic-phonon scattering and interface-roughness scattering. For the acoustic-phonon scattering, we calculate the scattering rates at temperature of 10 K by using the model proposed by Takagahara.⁵³ The differential scattering rates as functions of scattering angle θ and E_k are shown in Figs. 4(a) and 4(b) for emission and absorption processes, respectively. The scattering by acoustic-phonon emission prefers backward scattering, i.e., the maximum scattering rate is found for $\theta = \pi$. On the contrary, the acoustic-phonon absorption prefers forward scattering. Also, at low temperature, the scattering rate of emission is much larger than that of absorption.

In a semiconductor QW sample, the well width is not uniform due to the imperfection of each interface between well and barrier. Such a fluctuation introduces potential variations which influence the exciton dynamics, especially the lateral transport process. The structure of the fluctuation is characterized by a height Δ , which is normally assumed to be one or two monolayers,³⁸ and a lateral correlation length λ . Since we have no detailed information about the interface quality of the sample, in our simulation we take Δ to be one monolayer (0.283 nm) and use the λ as a free parameter to fit the experiments. Another choice would be to leave both of them as free parameters for the fitting. But this will make the fitting more unreliable due to the one more free parameter. Since the purpose of the simulation is to describe the general transport behavior of the excitons, rather than to extract the information of the interface structure of the sample, we

choose the first option. Thus, due to the uncertainty of the Δ used in the calculation, the fitted λ should not be used as a reliable number describing the interface structure. The interface-roughness scattering rates are calculated by using the method by Basu *et al.*⁵⁴ as shown in Fig. 4(c) as functions of scattering angle and E_k . For these curves, λ is set to be 3.7 nm, which is obtained by fitting the experiments. The directional property of the interface-roughness scattering depends strongly on the exciton energy. For hot excitons, the forward scattering is preferred, while the excitons with smaller energy are more likely to be scattered backward. This feature originates from the fact that the angular dependence of the differential scattering rate,

$$(1 - \cos \theta) \exp \left[-(\lambda k)^2 \sin^2 \frac{\theta}{2} \right], \quad (1)$$

where k represents the exciton wave vector, is composed of a forward factor and a backward factor. Thus, the λk determines the relative weight of these two factors.

The exciton-exciton scattering is neglected since the experiment is performed with low exciton density. The optical-phonon scattering is not included in our simulation since the exciton energy (9 meV) is too low for an optical-phonon emission and the optical-phonon absorption is negligible at the sample temperature of 10 K. For the recombination process, we assume that the exciton can recombine if its kinetic energy is smaller than the spectral linewidth (2.9 meV), and the recombination rate Γ is independent of the energy within this recombination window.⁵⁵ In this simulation, Γ is used as a second free parameter to fit the experiments. Although, the investigated samples are multiple QW's based on the polar material ZnSe, the influence of the polariton formation on the transport process is not included in the simulation. This is based on the fact that similar transport properties were observed in cw experiments from both single-QW and multiple-QW samples.⁵⁶ Also in the present time-resolved experiments, we observe similar transport behaviors from two multiple-QW samples with different barrier materials as well as different periods of QW.

At the beginning of the simulation, an ensemble of excitons is generated by the program. The position of each exciton is defined by random numbers such that the overall spatial distribution of the excitons coincides with the profile of the laser spot used in the experiment. The kinetic energy of the excitons is 9 meV according to the experiment condition, and the direction of the velocity of each exciton is selected randomly within the QW plane. Since the width of the laser pulse (150 fs) is much shorter than the temporal resolution of our study, the excitons are assumed to be generated simultaneously. After generation, the exciton travels in QW plane according to its velocity until it is scattered. The length of this "free flight" duration is selected by a random number generated according to the total scattering rate of all scattering processes considered. Then one of the scattering process is chosen to happen, according to the relative scattering rate among these processes. According to the type of the scattering process selected, we can determine the state of the exciton after this scattering event. This state is used as the initial

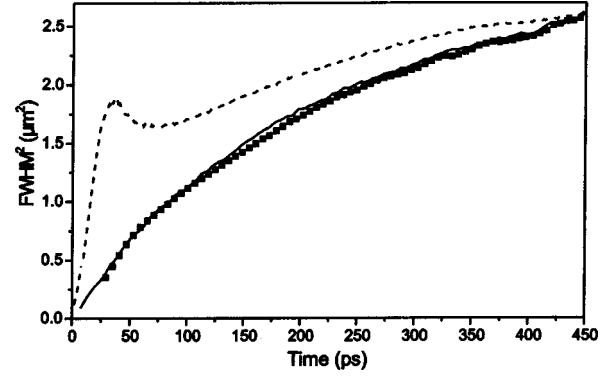


FIG. 5. Temporal evolution of the L^2 for Gaussian fits to measured photoluminescence profiles (squares), the Monte Carlo simulated photoluminescence profiles (solid line), and the Monte Carlo simulated total exciton population (dashed line).

state of the next "free flight." The above procedure is repeated many times until the radiative recombination takes place which terminates the existence of this exciton. In the simulation, an ensemble of 30 million excitons is simulated by this method.

IV. DISCUSSION

As we have discussed, the hot-exciton effects are typically neglected in the PL investigations on excitonic transport in QW. In the absence of hot-exciton effects, the exciton population $n(\vec{r}, t)$ obeys the two-dimensional diffusion equation

$$\frac{\partial n(\vec{r}, t)}{\partial t} = D \nabla^2 n(\vec{r}, t) - \frac{n(\vec{r}, t)}{\tau}, \quad (2)$$

with a constant diffusivity D .⁸ The last term describes the exciton recombination with a lifetime τ . Also, the measured PL $I(\vec{r}, t)$ is equivalent with the exciton population, i.e. $I(\vec{r}, t) \propto n(\vec{r}, t)$, since all of the excitons are in the recombination window. Based on these assumptions, the measured temporal evolution of the full width at half maxima (FWHM), say L of the PL profile obeys⁸

$$L^2(t) = L^2(t=0) + 16 \ln 2 D t. \quad (3)$$

That is, the square of the FWHM increases linearly with time with a slope being proportional to D .

To compare our experiments with the above formula, we fit the measured PL profiles in Fig. 3 by Gaussian functions (not shown in this figure) to get the FWHM's. The obtained temporal evolution of the L^2 is shown in Fig. 5 as the squares. We find a strong deviation from a linear function, namely, a sublinear rise of the L^2 in the time-range up to 400 ps. This result shows that the excitonic transport cannot be assumed as a classical diffusion. It implies the importance of the hot-exciton effects.

Beside the nonlinear expansion observe here, we have other evidences for the important role the hot exciton plays. From a temporally resolved PSB experiment, we have directly observed that the hot excitons remain nonthermal on a 100 ps time scale in ZnSe QW's.²⁹ This time scale is long

enough for significant transport to take place. We have also found from a spatially resolved cw PSB measurements that a nonthermal distribution of hot excitons can still be observed after a transport of $1.3 \mu\text{m}$.⁵⁷ From a cw measurement on the zero-phonon line of the PL, we have revealed the importance of the excitonic kinetic energy on the transport process.⁵⁶ These results together with the nonlinear expansion observed here by μ -TRPL strongly suggest that the hot excitons, rather than the relaxed excitons, dominate the transport.

We want to discuss now the detailed results of the MC simulation of the hot-exciton transport. As discussed in the preceding section, two free parameters, the correlation length of the interface roughness λ and recombination rate Γ , are used in the simulation to fit the experiment. As anticipated, these two parameters are relatively independent. With other conditions fixed, λ affects the spatial distribution of the PL, but has little influence on the temporal evolution. The opposite is true for Γ . With $\Gamma = 5.7 \times 10^9/\text{s}$, the PL decay is fitted satisfactorily (not shown here). The best fit of the spatial distribution is obtained when $\lambda = 3.7 \text{ nm}$, as shown in Fig. 3. Please note that the solid lines in this figure are not the just mentioned Gaussian fits to the experimental data, but are obtained by MC simulation of the excitonic dynamics. Figure 5 provides a more quantitative comparison of the experiment (squares) and the simulation (solid line) in terms of FWHM. It is remarkable that a perfect agreement is achieved by adjusting only one parameter, λ . This fact also confirms the validity of our model.

Beside its ability to reproduce the directly observable experimental results, the simulation also provides us a deeper insight into the underlying carrier dynamics. From the simulation, one can extract many aspects of the process that are not accessible in experiments. Figure 6(a) shows the temporal evolution of the average kinetic energy of excitons obtained from the simulation. The energy relaxation from the initial value (9 meV) to the thermal energy is clearly observed. We find the excitons remain hot up to about 400 ps. This is consistent with the sublinear increase of the L^2 up to 400 ps observed in Fig. 5, and confirms again that the excitonic transport on a time scale of several hundreds of picoseconds cannot be described as a classical diffusion with a constant D . After 400 ps, the relaxed excitons show the features of diffusive transport. On this regime, interface roughness can localize the relaxed excitons and can result in a subdiffusive transport.⁵⁸ Since the PL decay time is measured as 205 ps (Fig. 2), only a small fraction of the exciton ensemble can reach this regime. So these effects have minor influence on the excitonic transport studied here under non-resonant excitation.

If what we proved above were the only problem existing in previous PL investigations on excitonic transport, one could modify the diffusion model to fix this problem by simply substituting the constant diffusivity D by an effective diffusivity varying with time, $D_{\text{eff}}(t)$.⁹ One could even extract $D_{\text{eff}}(t)$ from the measured PL expansion by applying Eq. (3) to intervals, which are so small that the energy variation is negligible. However, a second problem arises from the hot-exciton effects, as we mentioned in the introduction and

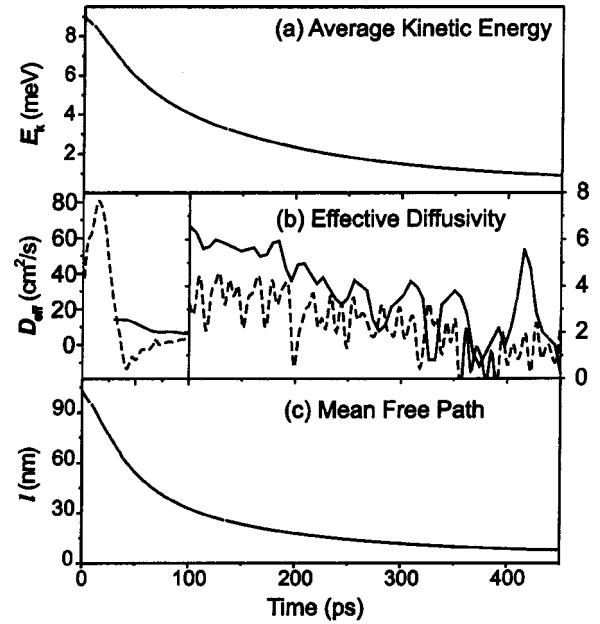


FIG. 6. Average kinetic energy (a), effective diffusivity (b), and mean-free path (c) of the excitons as functions of time. The effective diffusivity is obtained by modeling the $I(\vec{r}, t)$ (solid line) or $n(\vec{r}, t)$ (dashed line) with the modified diffusion model, respectively. Note that different vertical scales are used for different time-ranges in (b).

will demonstrate in the following that such a modified model is still invalid in describing the PL expansion.

The problem is, that the measured PL $I(\vec{r}, t)$ is not equivalent to the exciton population $n(\vec{r}, t)$ due to the invisibility of hot excitons in these techniques. Since a large portion of the exciton ensemble populates high kinetic-energy states, i.e. dark states, during the relaxation, this is quite obvious. Nevertheless, this problem is typically neglected.^{14–24} From our simulation, we find that during the relaxation, the $n(\vec{r}, t)$ is significantly different from the measured $I(\vec{r}, t)$, as shown in Fig. 3. In other words, the spatial distributions of excitons shown as the dashed lines in Fig. 3 can result in a narrower PL profile as shown by the solid lines. In Fig. 5, this difference is revealed in a quantitative way. The L^2 of the $n(\vec{r}, t)$ (dashed line) is significantly larger than that of $I(\vec{r}, t)$ (solid line) within about 400 ps. This can be understood by the fact that the hot excitons with high velocity can travel out of the excitation spot quite fast, but they are not visible in the spectrum.

In Fig. 5, we find a striking peak around 30 ps. This peak implies a breathing of the spatial distribution of the hot excitons. That is, in average, the hot excitons initially travel out of the excitation spot, then move back for a while until they go outward again. Such an oscillation is in striking contrast to the model of a classical diffusion, and can be understood according to the directional property of acoustic-phonon scattering. According to the differential scattering rates shown in Fig. 4(a), the scattering of acoustic-phonon emission prefers a backward scattering. Initially, the hot excitons are generated with an outward velocity in average. During

their traveling, interface-roughness scattering events can happen. Since in this transport regime, the energy of the excitons is still high (9 meV), the direction of the velocity is only slightly changed due to the forward-scattering character of interface roughness for hot excitons [Fig. 4(c)]. As soon as an acoustic-phonon scattering event happens, the direction of the velocity is most likely reversed. Then the excitons in an average move toward the excitation spot, resulting in the peak observed in Fig. 5. The next acoustic-phonon scattering event changes the direction of the velocity again. However, since the scattering events happen to each exciton in a random manner, the oscillating feature is averaged out after few scattering events. So, only one peak is observed in Fig. 5. We are aware of the fact, that we are not giving an experimental proof for the occurrence of the oscillations found in the MC simulations. But, the important message is here: when such oscillations of the hot-exciton population happen, they are not detectable in a standard PL experiment under nonresonant excitation.

To confirm quantitatively the invalidity of the modified diffusion model in describing the PL expansion, we compare in Fig. 6(b) the curves of $D_{\text{eff}}(t)$ extracted by modeling $I(\vec{r}, t)$ (solid line) or $n(\vec{r}, t)$ (dashed line) with the modified diffusion model, respectively. We find the curves to be quite different, especially in the first 100 ps. The $D_{\text{eff}}(t)$ obtained from $n(\vec{r}, t)$ increases rapidly in about 30 ps then drops to a negative value. This feature is induced by the breathing of the hot-exciton population. The difference between these two curves becomes smaller as the hot excitons relax toward the band minimum. After about 400 ps, the two curves overlap,

indicating that the excitons are thermalized. This is consistent with the energy relaxation process obtained from the simulation, as shown in Fig. 6(a).

From the simulation, we also extract the mean-free path (l) for each exciton. Figure 6(c) shows the temporal evolution of the averaged l of the whole ensemble. Since the rate of the interface-roughness scattering is larger than that of acoustic-phonon scattering, the l is governed by the interface-roughness scattering. During the energy relaxation, the exciton velocity decreases. Also, the interface-roughness scattering rate increases with the decreasing exciton energy. These two factors induce the decrease of l with time. We note that initially the mean-free path is nearly 100 nm, reflecting the ballistic transport right after the hot-exciton generation.

V. CONCLUSION

In conclusion, we show by μ -TRPL and MC simulation that the excitonic transport in ZnSe QW's at low temperature is dominated by hot excitons. Consequently, the two basic assumptions in previous PL investigations on excitonic transport: (i) the description by classical diffusion as well as (ii) the equivalence between the total exciton population and the measured PL profiles, are not valid in low-temperature experiments.

ACKNOWLEDGMENTS

This work was supported by the Deutsche Forschungsgemeinschaft (DFG) within Grant No. Ka 761/10-1 and within the DFG-Center for Functional Nanostructures (CFN).

-
- ¹J. Hegarty, L. Goldner, and M.D. Sturge, Phys. Rev. B **30**, 7346 (1984).
 - ²K. Hattori, T. Mori, H. Okamoto, and Y. Hamakawa, Appl. Phys. Lett. **51**, 1259 (1987).
 - ³H. Schwab, K.-H. Pantke, J.M. Hvam, and C. Klingshirn, Phys. Rev. B **46**, 7528 (1992).
 - ⁴J. Erland, B.S. Razbirin, K.-H. Pantke, V.G. Lyssenko, and J.M. Hvam, Phys. Rev. B **47**, 3582 (1993).
 - ⁵D. Oberhauser, K.-H. Pantke, J.M. Hvam, G. Weimann, and C. Klingshirn, Phys. Rev. B **47**, 6827 (1993).
 - ⁶V. Mizeikis, V.G. Lyssenko, J. Erland, and J.M. Hvam, Phys. Rev. B **51**, 16 651 (1995).
 - ⁷A.C. Schaefer, J. Erland, and D.G. Steel, Phys. Rev. B **54**, 11 046 (1996).
 - ⁸L.M. Smith, D.R. Wake, J.P. Wolfe, D. Levi, M.V. Klein, J. Klem, T. Henderson, and H. Morkoç, Phys. Rev. B **38**, 5788 (1988).
 - ⁹H.W. Yoon, D.R. Wake, J.P. Wolfe, and H. Morkoç, Phys. Rev. B **46**, 13 461 (1992).
 - ¹⁰M. Achermann, B.A. Nechay, F. Morier-Genoud, A. Schertel, U. Siegner, and U. Keller, Phys. Rev. B **60**, 2101 (1999).
 - ¹¹F.A. Majumder, H.-E. Swoboda, K. Kempf, and C. Klingshirn, Phys. Rev. B **32**, 2407 (1985).
 - ¹²L.M. Smith, J.S. Preston, J.P. Wolfe, D.R. Wake, J. Klem, T. Henderson, and H. Morkoç, Phys. Rev. B **39**, 1862 (1989).
 - ¹³B.A. Nechay, U. Siegner, F. Morier-Genoud, A. Schertel, and U. Keller, Appl. Phys. Lett. **74**, 61 (1999).
 - ¹⁴H. Hillmer, A. Forchel, S. Hansmann, M. Morohashi, E. Lopez, H.P. Meier, and K. Ploog, Phys. Rev. B **39**, 10 901 (1989).
 - ¹⁵H. Hillmer, A. Forchel, and C.W. Tu, Phys. Rev. B **45**, 1240 (1992).
 - ¹⁶H. Akiyama, T. Matsusue, and H. Sakaki, Phys. Rev. B **49**, 14 523 (1994).
 - ¹⁷H. Hillmer, S. Hansmann, A. Forchel, M. Morohashi, and E. Lopez, Appl. Phys. Lett. **53**, 1937 (1988).
 - ¹⁸H. Hillmer, A. Forchel, R. Sauer, and C.W. Tu, Phys. Rev. B **42**, 3220 (1990).
 - ¹⁹Y. Takahashi, K. Muraki, S. Fukatsu, S.S. Kano, Y. Shiraki, and R. Ito, Jpn. J. Appl. Phys. **32**, 5586 (1993).
 - ²⁰Y. Takahashi, K. Muraki, S. Fukatsu, S.S. Kano, Y. Shiraki, and R. Ito, Solid State Commun. **88**, 677 (1993).
 - ²¹L.-L. Chao, G.S. Gargill III, E. Snoeks, T. Marshall, J. Petruzzello, and M. Pashley, Appl. Phys. Lett. **74**, 741 (1999).
 - ²²A.F.G. Monte, S.W. da Silva, J.M.R. Cruz, P.C. Morais, and A.S. Chaves, Phys. Rev. B **62**, 6924 (2000).
 - ²³A.F.G. Monte, S.W. da Silva, J.M.R. Cruz, P.C. Morais, and H.M. Cox, J. Appl. Phys. **85**, 2866 (1999).
 - ²⁴A.F.G. Monte, S.W. da Silva, J.M.R. Cruz, P.C. Morais, and H.M. Cox, Physica B **273/274**, 963 (1999).
 - ²⁵A. Vertikov, I. Ozden, and A. Nurmikko, Appl. Phys. Lett. **74**, 850 (1999).

- ²⁶F.P. Logue, D.T. Fewer, S.J. Hewlett, J.F. Heffernan, C. Jordan, P. Rees, J.F. Donegan, E.M. McCabe, J. Hegarty, S. Taniguchi, T. Hino, K. Nakano, and A. Ishibashi, *J. Appl. Phys.* **81**, 536 (1997).
- ²⁷A. Vertikov, I. Ozden, and A.V. Nurmikko, *J. Appl. Phys.* **86**, 4697 (1999).
- ²⁸V. Malyarchuk, J.W. Tomm, V. Talalaev, Ch. Lienau, F. Rinner, and M. Baeumler, *Appl. Phys. Lett.* **81**, 346 (2002).
- ²⁹M. Umlauff, J. Hoffmann, H. Kalt, W. Langbein, J.M. Hvam, M. Scholl, J. Söllner, M. Heuken, B. Jobst, and D. Hommel, *Phys. Rev. B* **57**, 1390 (1998).
- ³⁰D.S. Citrin, *Phys. Rev. Lett.* **69**, 3393 (1992).
- ³¹M. Vollmer, H. Giessen, W. Stolz, W.W. Rühle, L. Ghislain, and V. Elings, *Appl. Phys. Lett.* **74**, 1791 (1999).
- ³²S. Moehl, H. Zhao, B. Dal Don, S. Wachter, and H. Kalt, *J. Appl. Phys.* (to be published).
- ³³C. Jacoboni and P. Lugli, *The Monte Carlo Method for Semiconductor Device Simulation* (Springer, New York, 1989).
- ³⁴P. Lugli and S.M. Goodnick, *Phys. Rev. Lett.* **59**, 716 (1987).
- ³⁵M. Artaki and K. Hess, *Phys. Rev. B* **37**, 2933 (1988).
- ³⁶J.L. Educato and J.P. Leburton, *Phys. Rev. B* **49**, 2177 (1994).
- ³⁷M. Mosko, A. Mosková, and V. Cambel, *Phys. Rev. B* **51**, 16 860 (1995).
- ³⁸Y. Takahashi, *Phys. Rev. B* **53**, 7322 (1996).
- ³⁹S.D. Baranovskii, R. Eichmann, and P. Thomas, *Phys. Rev. B* **58**, 13 081 (1998).
- ⁴⁰A.V. Shchegrov, D. Birkedal, and J. Shah, *Phys. Rev. Lett.* **83**, 1391 (1999).
- ⁴¹S. Barbieri, F. Beltram, and F. Rossi, *Phys. Rev. B* **60**, 1953 (1999).
- ⁴²T.C. Damen, J. Shah, D.Y. Oberli, D.S. Chemla, J.E. Cunningham, and J.M. Kuo, *Phys. Rev. B* **42**, 7434 (1990).
- ⁴³P.W.M. Blom, P.J. van Hall, C. Smit, J.P. Cuypers, and J.H. Wolter, *Phys. Rev. Lett.* **71**, 3878 (1993).
- ⁴⁴I.-K. Oh, J. Singh, A. Thilagam, and A.S. Vengurlekar, *Phys. Rev. B* **62**, 2045 (2000).
- ⁴⁵K. Siantidis, V.M. Axt, and T. Kuhn, *Phys. Rev. B* **65**, 035303 (2002).
- ⁴⁶M. Gulia, F. Rossi, E. Molinari, P.E. Selbmann, and P. Lugli, *Phys. Rev. B* **55**, 16 049 (1997).
- ⁴⁷M. Gurioli, P. Borri, M. Colocci, M. Gulia, F. Rossi, E. Molinari, P.E. Selbmann, and P. Lugli, *Phys. Rev. B* **58**, 13 403 (1998).
- ⁴⁸R.P. Stanley, J. Hegarty, R. Fischer, J. Feldmann, E.O. Göbel, R.D. Feldman, and R.F. Austin, *Phys. Rev. Lett.* **67**, 128 (1991).
- ⁴⁹N. Pelekanos, J. Ding, Q. Fu, A.V. Nurmikko, S.M. Durbin, M. Kobayashi, and R.L. Gunshor, *Phys. Rev. B* **43**, 9354 (1991).
- ⁵⁰J.H. Collet, H. Kalt, L.S. Dang, J. Cibert, K. Saminadayar, and S. Tatarenko, *Phys. Rev. B* **43**, 6843 (1991).
- ⁵¹H. Zhao, S. Moehl, and H. Kalt, *Phys. Rev. Lett.* **89**, 097401 (2002).
- ⁵²H. Kalt, M. Umlauff, J. Hoffmann, W. Langbein, J.M. Hvam, M. Scholl, J. Söllner, M. Heuken, B. Jobst, and D. Hommel, *J. Cryst. Growth* **184/185**, 795 (1998).
- ⁵³T. Takagahara, *Phys. Rev. B* **31**, 6552 (1985).
- ⁵⁴P.K. Basu and P. Ray, *Phys. Rev. B* **44**, 1844 (1991).
- ⁵⁵J. Feldmann, G. Peter, E.O. Göbel, P. Dawson, K. Moore, C. Foxon, and R.J. Elliott, *Phys. Rev. Lett.* **59**, 2337 (1987).
- ⁵⁶H. Zhao, S. Moehl, S. Wachter, and H. Kalt, *Appl. Phys. Lett.* **80**, 1391 (2002).
- ⁵⁷H. Zhao, S. Moehl, and H. Kalt, *Appl. Phys. Lett.* **81**, 2794 (2002).
- ⁵⁸B. Hanewinkel, A. Knorr, P. Thomas, and S.W. Koch, *Phys. Rev. B* **60**, 8975 (1999).